Retrieval and analysis of Arctic albedo from NOAA/AVHRR data

WANG Hongyan, GUAN Lei, KANG Liting

Ocean Remote Sensing Institute/Department of Marine Technology, College of Information Science and Engineering, Ocean University of China, Qingdao 266100, *China*

Abstract: Surface albedo in the Arctic is one of the most important factors influencing the polar heat budget. The impact of variations of the Arctic sea ice albedo on the heat budget of the earth-atmosphere system and on global climate change is significant. In this paper, the surface albedo in the Arctic was derived using the Level-1B (L1B) data from the advanced very high resolution radiometer (AVHRR) onboard the National Oceanic and Atmospheric Administration (NOAA) polar-orbiting satellites. We applied narrow-to-broadband conversion, anisotropic correction, atmospheric correction, and cloud detection to the satellite data, and obtained broadband surface albedo products in clear conditions with a 4 km spatial resolution. Comparisons between the AVHRR albedo products and in situ measurements collected during the Surface Heat Budget of the Arctic Ocean (SHEBA) project showed a bias of −0.07 and a standard deviation of 0.05 during the spring-winter season. Monthly averaged NOAA/AVHRR surface albedo data from 2008 to 2010, combined with in situ measurements from the fourth Chinese Arctic research expedition, were used to study the variation of the Arctic sea ice albedo. The influence of snowfall and ice ridges on the variation of surface albedo was analyzed. The albedo decreased significantly and rapidly by about 0.3 when the snow was melting. Comparing between the albedo variations in the rough multi-year ice area and smooth first-year ice area shows an albedo difference of 0.2 during the melting season. The results indicate that the melting of snow and ice was the dominant factor for the variation of the Arctic albedo.

Key words: NOAA/AVHRR, Arctic, albedo, snowfall, ice ridge

CLC number: TP79 **Document code:** A

Citation format: **Wang H Y, Guan L and Kang L T. 2013. Retrieval and analysis of Arctic albedo from NOAA/AVHRR data. Journal of Remote Sensing, 17(3): 541−552**

1 INTRODUCTION

Surface albedo is one of the most important factors influencing the radiation budget of the earth-atmosphere system (Curry, et al., 1996; Stamnes, et al., 1999), but for Arctic sea ice, the albedo takes on an added significance with model results indicating that a 0.15—0.20 decrease in the summer albedo would lead to a complete disappearance of perennial sea ice (Maykut & Untersteiner, 1971). The sea ice-albedo positive feedback (Budyko, 1969; Sellers, 1969; Schlesinger & Jiang, 1988) exemplifies the strong connection between sea ice cover and climate. As temperatures increase, the extent of snow and ice is reduced, decreasing the surface albedo and increasing the amount of sunlight that is absorbed by the earth-atmosphere system (Curry, et al., 1995). The effect leads to further melting of sea ice. The arctic sea ice-albedo positive feedback amplifies global warming; therefore, it is important to monitor the variation of polar sea ice albedo.

Albedo is defined as the ratio of the upwelling solar irradiance, integrated over all solar wavelengths, divided by the total downwelling irradiance also integrated over all solar wavelengths (Valiente, et al., 1995; Song & Gao, 1999). This definition is different from reflectance. Reflectance is the fraction of incident radiation reflected by the surface and is generally treated as a directional property that is a function of the reflected direction, the incident direction, and the incident wavelength. Hence, albedo is the integral of the reflectance in all directions. It is the most important surface parameter retrieved by remote sensing data and a physical parameter used to describe the property of surface reflectance of solar radiation (Wang & Gao, 2004). There are two methods to obtain the albedo data; one is from in situ measurements and the other is from satellite observations. Visible and infrared sensors are used for observations of snow and ice albedo. Albedo measurements over snow and ice are retrieved based on the radiative transfer model. Satellite data can be an important tool for obtaining the albedo since these measurements provide extensive spatial and temporal coverage. However, the data is limited by the narrow spectral range of the radiometer and the limited viewing angle. Thus, it is necessary to convert the narrowband albedo to broadband albedo (Jiang, 2006; Brandt, et al., 2005; De Abreu, et al., 1994; Valiente, et al., 1995; Song & Gao, 1999; Xiong, et al., 2002).

Received: 2012-02-14; **Accepted:** 2012-09-05; **Version of record first published:** 2012-09-12

Foundation: National High Technology Research and Development Program of China (863 program) (No. 2008AA121701)

First author biography: WANG Hongyan (1984—), female, Ph. D. candidate. His research focuses on visible-infrared satellite ocean remote sensing. E-mail: wanghongyan2011@gmail.com

Corresponding author biography: GUAN Lei (1969—), female, professor. Her research focuses on satellite ocean remote sensing. E-mail: leiguan@ouc.edu.cn

2 DATA

2.1 Satellite data

The NOAA/AVHRR Global Area Coverage (GAC) data with a spatial resolution of 4.4 km were downloaded from the Comprehensive Large Array-data Stewardship System (CLASS). There are typically 14 satellite passes each day. The specifications of AVHRR are shown in Table 1. CLASS is an electronic library of NOAA environmental satellite data. The datasets are available from [2008-01-09] http://www.nsof.class.noaa.gov/saa/products/welcome.

Table 1 Specifications of AVHRR

Parameters	1	2	3A	3B	4	5
Spectral range/μm	0.58—0.68	0.725—1.000	1.58—1.64	3.55—3.93	10.3—11.3	11.5—12.5
S/N(0.5% albedo)	≥9:1	≥9:1	≥20:1	—	—	—
NE△T (300 K)	—	—	—	≤0.12 K	≤0.12 K	≤0.12 K
Temperature range/K	—	—	—	108—335	180—335	180—335

The Special Sensor Microwave Imager (SSM/I) global ice concentration and snow extent product are the auxiliary data for the AVHRR albedo retrieval. The data were delivered by the National Snow and Ice Data Center (NSIDC) with a spatial resolution of 25 km (Nolin, et al., 1998). The dataset is available from: [2008-01-09] http://nsidc.org/data/docs/daac/nise1_nise.gd.html#format.

The Advanced Microwave Scanning Radiometer-Earth Observing System (AMSR-E) snow depth products were delivered by NSIDC with a spatial resolution of 12.5 km (Cavalieri, et al., 2004). This dataset is available from: [2008-01-09] http://nsidc.org/data/ae_si12.html.

2.2 In situ observations

2.2.1 In situ data from the fourth Chinese arctic research expedition

The in situ data were obtained during the forth Chinese Arctic research expedition in 2010. The 82-day expedition was carried out by M/V *Xue Long*. The voyage covered 12600 nautical miles and reached 88°26′N (Yu, 2011). During the experiment, albedo measurements were made using a Kipp & Zonen CMA6 albedometer at short- and long-term stations for about 22 days from July 27th to August 24th, 2010.

The albedo measurements at the short-term stations were made mainly for snow melt and melt ponds. For the measurements of sea ice albedo, a smooth surface, with no melt ponds or ridges was chosen. For melt ponds, the CMA6 albedometer was deployed in the middle of the melt pond, farthest from the edge of the ponds.

At the long-term stations, measurements of snow depth and albedo were carried out. The albedo measurements were made every 20 m along 200 × 125 m cross lines every four days.

2.2.2 SHEBA data

The Canadian Coast Guard icebreaker Des Groseilliers began a year-long drift of the ice station Surface Heat Budget of the Arctic Ocean (SHEBA). The SHEBA ice floe drifted more than 1400 km in the Beaufort and Chukchi Seas with latitude varying from 74°N to 81°N (Perovich, et al., 1999a; Persson, et al., 2002). The albedo measurements were monitored using a Kipp & Zonen albedometer at a wide variety of sites selected to include all available multi-year ice types and conditions. Albedo measurements were made every 2.5 m along a 200 meter long albedo line from October 1997 to October 1998 with an accuracy of ±0.01 (Perovich, et al., 1999a; Perovich, et al., 1999b; Perovich, et al., 2002). The dataset is available from: [2010-09-10] ftp://ftp1.esrl.noaa.gov/users/opersson/sheba/.

2.3 Study area

A 200 × 200 km area centered at the location (75°N, 147°W; point A in Fig. 1) was selected to study the variation of albedo with snowfall. The NSIDC AMSR-E snow depth products were used.

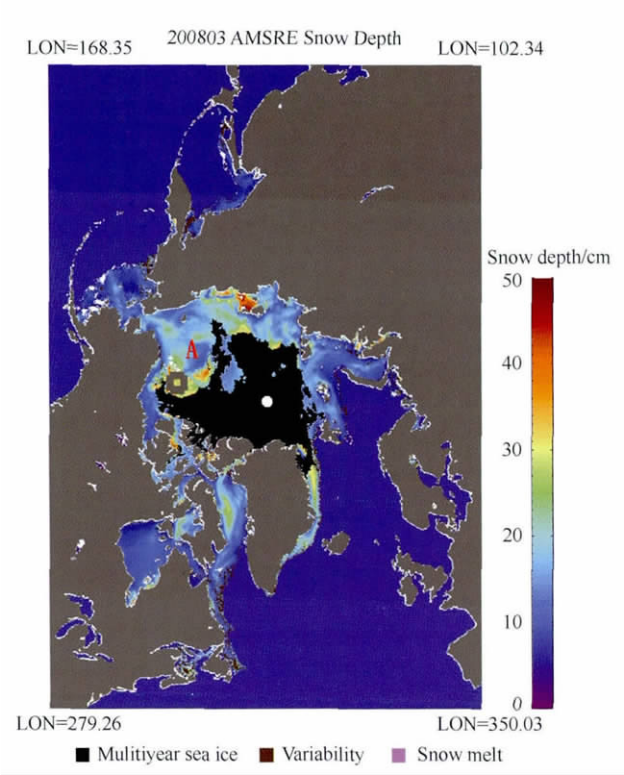

Fig. 1 Monthly averaged snow depth for March 2008 ("A" indicates the study area)

Two 200 × 200 km areas were selected in the Beaufort Sea (75°N, 128°W) and Chukchi Sea (72°N, 166°W) to study the influence of ice ridges on albedo variation. Most of the Beaufort Sea was covered by multi-year sea ice with accumulated ice ridge. The surface was relatively rough and the snow was deep. The near-shore ice on the Chukchi Sea was smooth first-year sea ice but with small ice ridges (Sturm, et al., 2006). The location of the study areas are shown in Fig. 2 where "A" indicates

the area selected in the Beaufort Sea and "B" is the area in the Chukchi Sea. The white areas in Fig. 2 indicate cloudy pixels or no valid satellite albedo data.

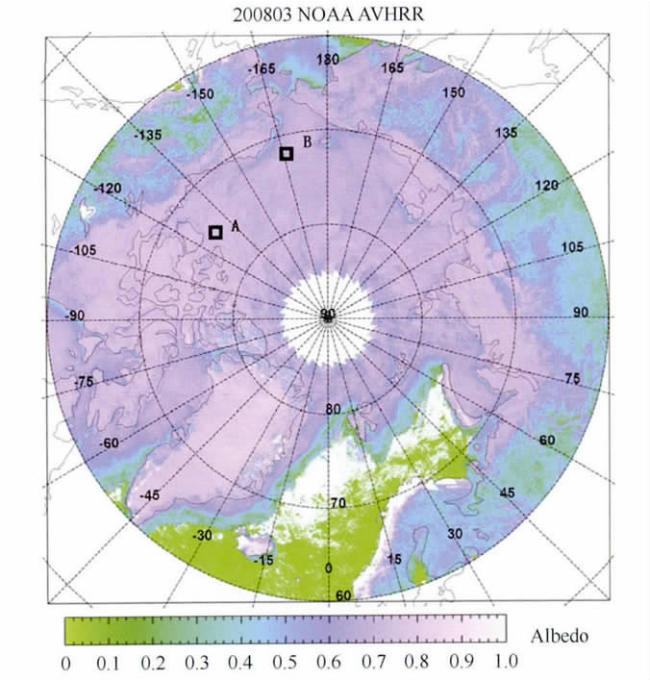

Fig. 2 Monthly averaged albedo for March 2008 in the Arctic (A—Beaufort Sea region; B—Chukchi Sea region)

3 DATA PROCESSING

A linear relationship between the narrowband surface albedo and the Top of the Atmosphere (TOA) reflectance was d erived for AVHRR channels 1 and 2 by Koepke (1989). Different coefficients were used for different aerosol optical depths, o zone and water vapor amounts, and solar zenith angles. Koepke's method had been applied to derive the surface albedo from AVHRR data (De Abreu, et al., 1994; Knap & Oerlemans, 1996; Knap, et al., 1999; Stroeve, et al., 1997; Li & Leighton, 1992; Lindsay & Rothrock, 1994). In this study, solar zenith angle correction, narrow-to-broadband conversion, anisotropic correction, atmospheric correction (Fowler, et al., 2000), and cloud detection (Key, 1999) were applied for the albedo retrievals.

The TOA reflectance was derived from the AVHRR visible and near-infrared channels (0.58—0.68 μm and 0.725—1.000 μm) by solar zenith angle correction.

$$R_{1,\mathrm{toa}} = r_1/\cos(\theta) \quad (1)$$

$$R_{2,\mathrm{toa}} = r_2/\cos(\theta) \quad (2)$$

where $R_{1,\mathrm{toa}}$, $R_{2,\mathrm{toa}}$ are TOA reflectance channels 1 and 2, r_1 and r_2 are the percent reflectance for channels 1 and 2, and θ is the solar zenith angle.

The broadband reflectance was derived from the TOA r eflectance by narrowband to broadband conversion.

$$R_{\mathrm{toa}} = a + b \cdot R_{1,\mathrm{toa}} + c \cdot R_{2,\mathrm{toa}} \quad (3)$$

where R_{toa} is the broadband TOA reflectance and a, b, and c are the regression coefficients. The radiative transfer model Streamer was used to simulate the TOA reflectance regression relationship over a broad range of viewing and illumination angles, atmospheric conditions, and surface types and albedos (Key & Schweiger, 1998). When the surface is covered by sea ice the r eflectance is

$$R_{\mathrm{toa}} = 0.022 + 0.277R_{1,\mathrm{toa}} + 0.507R_{2,\mathrm{toa}} \quad (4)$$

Next, the anisotropic correction was applied.

$$A_{\mathrm{toa}} = R_{\mathrm{toa}}/f \quad (5)$$

where A_{toa} is the TOA albedo and f is the anisotropic reflectance factor.

The clear condition surface broadband albedo was estimated with Eq. (6):

$$A_{\mathrm{surface}} = (A_{\mathrm{toa}} - m)/n \quad (6)$$

where A_{surface} is the surface broadband albedo. m and n depend on the water vapor, aerosol amounts, and solar zenith angle.

The cloud detection was applied based on the algorithm of the Cloud and Surface Parameter Retrieval System (CASPR) (Key, 1999). CASPR includes five cloud tests: (1) The split-w indow cirrus test (11—12 μm) was applied to ice, ocean, and land cover. (2) The warm cloud test (11—12 μm) was applied to all surface types. (3) The water cloud test (3.7 μm) was used to identify liquid water clouds over ocean and land. (4) The cold cloud test (11 μm) was designed to detect very cold clouds o-ver all the surface types. (5) The clear test was applied only to those pixels labeled cloudy by the cloud test for ice and snow surfaces. The result after the cloud detection is shown in Fig. 3.

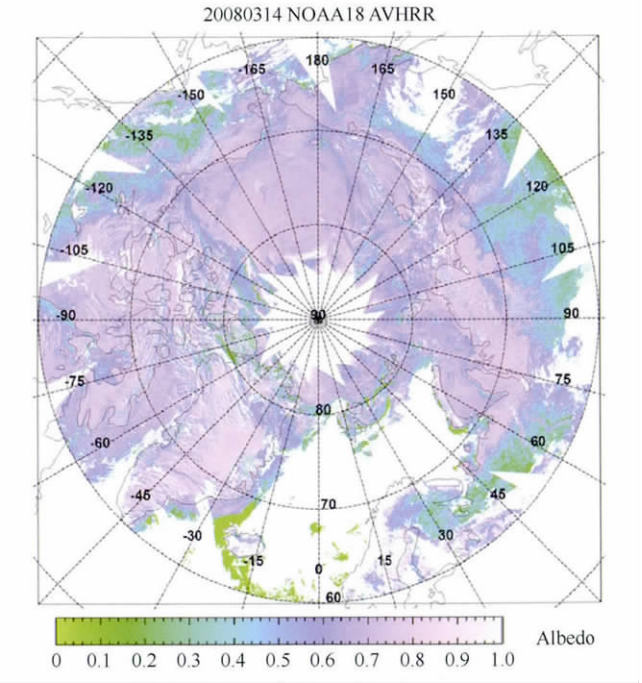

Fig. 3 Surface albedo on March 14th, 2008

Due to cloud influence there were no match-ups between the in situ measurements from the forth Chinese Arctic research expedition and the AVHRR albedo data. The historical data from SHEBA were used for the validation of the AVHRR albedo. A ccording to the records of the SHEBA field experiments, during April and May, when the surface consisted of dry snow, the surface albedo was 0.84. The melt season lasted a total of 80 days from late May to mid-August. The surface albedo reached a minimum value on August 12nd. Snow began to accumulate on the ice

in late August and by mid-September the snow cover was roughly 10 cm deep (Curry, et al., 2001). Match-ups were generated between the SHEBA and AVHRR albedo data during the frozen season and melt season with a spatial window of 4 km and temporal window of 2 h. The number of match-ups was 28; 22 match-ups in the frozen season and six in the melt season. The SHEBA and AVHRR match-up data plotted in Fig. 4 shows a bias of −0.07 and standard deviation of 0.05 in the frozen season. For the melt season, the differences of the six match-ups were between −0.23 and −0.08 and the bias was −0.17. The small difference in the frozen season was due to the uniform s urface type while the large difference in the melt season was due to the complicated surface type which was probably covered by several surface types such as melt snow and melt pond over the 4 km satellite window. This resulted in inconsistency in the surface types between the SHEBA field measurements and AVHRR observations. This spatial difference was the main reason for the big difference between the six match-ups in the melt season.

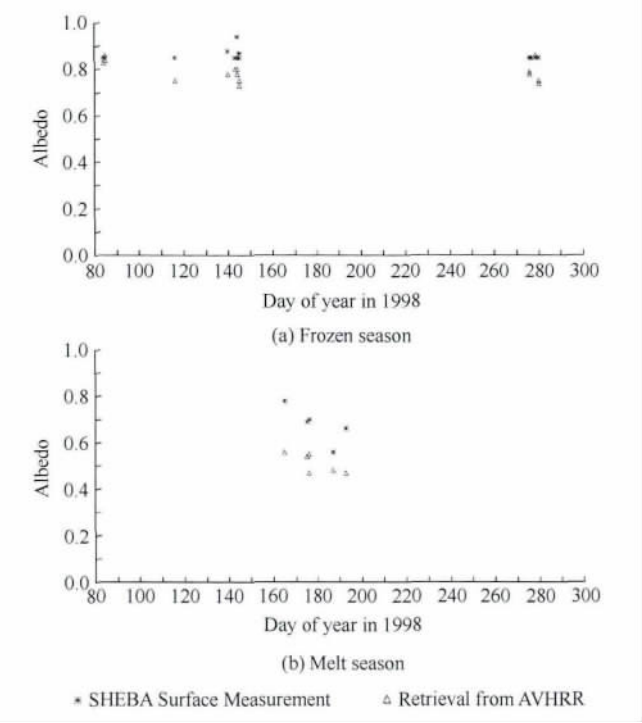

Fig. 4 Albedo validation

4 ANALYSIS OF ALBEDO VARIATION

The satellite data from 2008 to 2010 were processed by the methods described in Section 3, and monthly averaged AVHRR surface albedo data were obtained. This albedo data, combined with CMA6 measurements from the forth Chinese Arctic research expedition, were used to analyze the variation of the albedo in the Arctic area. There were five phases in the evolution of the albedo during the transition season (between May and A ugust) (Curry & Schramm, 1995; Laine, 2004; Perovich, et al., 2002; Xiong, et al., 2002). (1) Dry snow: in April and May the surface albedo was high (0.8—0.9) and the surface types were complicated. (2) Melt snow: by the end of May most of the snowfall had ceased, and the albedo decreased to the "aging snow" value. In the beginning of June the snow began to melt and the albedo decreased to the "melt snow" value. (3) Pond formation: in mid-July the snow melted and within one week the albedo decreased sharply because of pond formation. (4) Pond e volution: after phase (3) the snow continued to melt. All the snow had melted except over the thickest ice, leaving bare ice. The albedo reached its minimum when the melt pond area was at a maximum. (5) Autumn freeze up: in August, the melt ponds had refrozen and the albedo increased to the "bare ice" value. In September, the leads began to freeze and the snow began to a ccumulate; the albedo returned to the "new snow" value. The CMA6 data showed the variation of the albedo for different s urface types. The dry snow albedo was high (0.8—0.9), the melt snow albedo decreased to 0.6, and the melt pond albedo was a bout 0.1—0.2. Thus, the albedo decreased as the snow and ice melted—a trend which is consistent with the results of Lindsay and Rothrock (1994).

To investigate the relationship between snowfall and ice r idges and the albedo variation, two regions were selected. The averaged AVHRR albedo from 2008 to 2010 in area A (Fig. 1) were analyzed to investigate the relationship between snowfall and albedo variation. The result is shown in Fig. 5. During March and April when the snow and ice were frozen, the albedo was 0.7—0.8. By the end of May, the snow began to melt and the a lbedo decreased to 0.66—0.75. The albedo continued to decrease to 0.45 as the snow and ice melted and reached its m inimum value in August when the melt pond area reached its maximum. The ponds began to freeze in September and the albedo increased slowly. The rapid drop (by 0.3) in the albedo as the snow was melting is evident in all three datasets (2008—2010).

To investigate the ice ridge influence on albedo variation, the monthly-averaged AVHRR albedo from March to September 2009 in areas A and B (Fig. 2) was analyzed. The result is shown in Fig. 6. In March and April, when the surface was covered by snow and ice, the albedo in the two regions was 0.75. By the end of May, as the snow began to melt, the albedo at the Beaufort

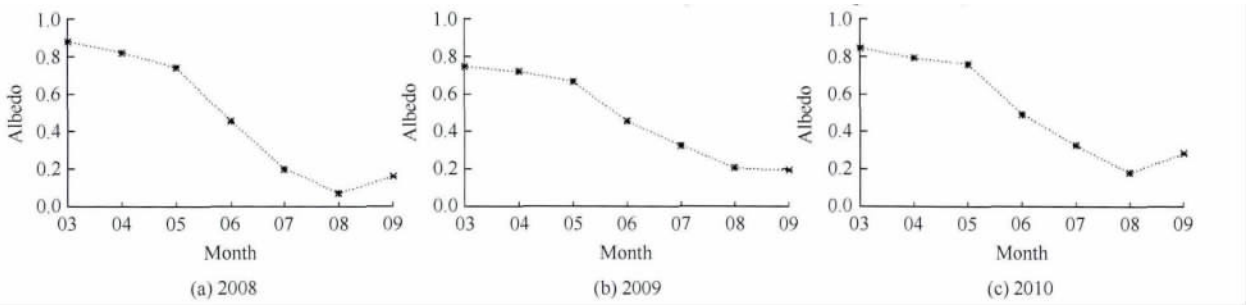

Fig. 5 Albedo variation in snowfall area from 2008 to 2010

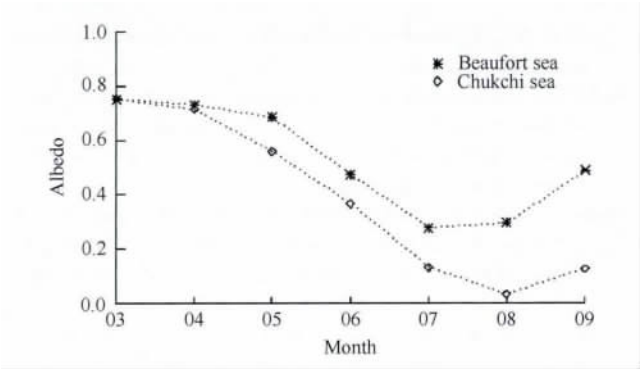

Fig. 6 Albedo variations in Beaufort sea region and Chukchi sea region in 2009

sea region decreased to 0.68 while in the Chukchi sea region it decreased to 0.56. In June, when the snow melted, the albedo in the Beaufort sea and Chukchi sea regions decreased to 0.47 and 0.37, respectively. In July, as the snow and ice melted, the albedo in the Beaufort and Chukchi seas continued to decrease, reaching 0.28 and 0.13, respectively. The albedo reached its m inimum when the melt pond area was at a maximum in August. The a lbedo increased when the melt ponds began to freeze in late September, then slowly decreased by 0.2 during the melting of the snow and ice.

5 CONCLUSION

In this paper, the broadband surface albedo products in clear conditions with a spatial resolution of 4 km were derived using NOAA/AVHRR GAC L1B data by narrow-to-broadband conversion, anisotropic correction, atmospheric correction, and cloud detection. The comparisons between the AVHRR albedo products and the SHEBA data show a bias of −0.07 and a standard deviation of 0.05 during the frozen season. The monthly-averaged NOAA/AVHRR surface albedo data from 2008 to 2010, combined with in situ observations from the forth Chinese Arctic research expedition, were used to study the variation of the Arctic sea ice albedo. The influence of snowfall and ice ridges on the variation of the surface albedo was analyzed. The albedo decreased significantly and rapidly by about 0.3 when the snow was melting. Comparing the albedo variations between the rough multi-year ice area and smooth first-year ice area shows an albedo difference of 0.2 between the two regions during the melting season. Our results indicate that the melting of snow and ice is the dominant factor for the variation of albedo in the A rctic.

Acknowledgements: The NOAA/AVHRR data were p rovided by CLASS, the SSM/I data and AMSR-E data were provided by NSIDC, and the albedo in situ observations data were obtained from the Forth Chinese Arctic Research Expedition and SHEBA.

REFERENCES

Brandt R E, Warren S G, Worby A P and Grenfell T C. 2005. Surface a lbedo of the Antarctic sea ice zone. Journal of Climate, 18(17): 3606 – 3622 [DOI: 10.1175/JCLI3489.1]

Budyko M I. 1969. The effect of solar radiation variations on the climate of the earth. Tellus, 21: 611 – 619

Cavalieri D J, Markus T and Comiso J. 2004. Updated daily. AMSR-E/Aqua Daily L3 12.5 km Brightness Temperature, Sea Ice Conentration, & Snow Depth Polar Grids V002, 2008—2010. Boulder, Colorado USA: National Snow and Ice Data Center. Digital media

Curry J A and Schramm J L. 1995. Sea ice-albedo climate feedback mechanism. Journal of Climate, 8(2): 240 – 247 [DOI: 10.1175/1520 – 0442(1995)008 < 0240: SIACFM > 2.0.CO; 2]

Curry J A, Rossow W B, Randall D and Schramm J L. 1996. Overview of Arctic cloud and radiation characteristics. Journal of Climate, 9(8): 1731 – 1764 [DOI: 10.1175/1520 – 0442(1996) 009 < 1731: OOACAR > 2.0.CO; 2]

Curry J A, Schramm J L, Perovich D K and Pinto J O. 2001. Applications of SHEBA/FIRE data to evaluation of snow/ice albedo parameterizations. Journal of Geophysical Research: Atmospheres, 106(D14): 15345 – 15355 [DOI: 10.1029/2000JD 900311]

De Abreu R A, Key J, Maslanik J A, Serreze M C and LeDrew E F. 1994. Comparison of in situ and AVHRR-derived broadband albedo over Arctic sea ice. Arctic, 47(3): 288 – 297

Fowler C, Maslanik J, Haran T, Scambos T, Key J and Emery W. 2000. AVHRR Polar Pathfinder twice-daily 5 km EASE-grid Composites. http://nsidc.org/data/nsidc-0066.html, Natl. Snow and Ice Data Cent., Boulder, Colo

Jiang X. 2006. Progress in the research of snow and ice albedo. Journal of Glaciology and Geocryology, 28(5): 728 – 736

Key J. 1999. The Cloud and Surface Parameter Retrieval (CASPR) System for Polar AVHRR. Cooperative Institute for Meteorological Satellite Studies. University of Wisconsin, Madison

Key J and Schweiger A J. 1998. Tools for atmospheric radiative transfer: *streamer* and *FluxNet*. Computers and Geosciences, 24(5): 443 – 451 [DOI: 10.1016/S0098 – 3004(97)00130 – 1]

Knap W H and Oerlemans J. 1996. The surface albedo of the Greenland ice sheet: satellite-derived and in situ measurement in the Sondre Stromfjord and during the 1991 melt season. Journal of Glaciology, 42: 364 – 374

Knap W H, Brock B W, Oerlemans J and Wills I C. 1999. Comparison of Landsat TM-derived and ground-based albedos of Hunt Glacier d'Arolla, Switzerland. International Journal of Remote Sensing, 20: 3293 – 3310

Koepke P. 1989. Removal of atmospheric effects from AVHRR albedos. Journal of Applied Meteorology, 28(12): 1344 – 1348 [DOI: 10.1175/1520 – 0450(1989)028 < 1341: ROAEPA > 2.0.CO; 2]

Laine V. 2004. Arctic sea ice regional albedo variability and trends. Journal of Geophysical Research, 109(C06027): 1982 – 1998 [DOI: 10.1029/2003JC001818]

Li Z Q and Leighton H G. 1992. Narrowband to broadband conversion with spatially autocorrelated reflectance measurement. Journal of Applied Meteorology, 31(5): 421 – 433 [DOI: 10.1175/1520 – 0450(1992)031 < 0421: NTBCWS > 2.0.CO; 2]

Lindsay R W and Rothrock D A. 1994. Arctic sea ice albedo from AVHRR. Journal of Climate, 7(11): 1737 – 1749 [DOI: 10.1175%2f1520 – 0442(1994)007%3c1737%3aASIAFA%3e2.0.CO%3b2]

Maykut G A and Untersteiner N. 1971. Some results from a time dependent, thermodynamic model of sea ice. Journal of Geophysical Research, 76(6): 1550 – 1575 [DOI: 10.1029/JC076i006p01550]

Nolin A, Armstrong R L and Maslanik J. 1998. Updated daily. Near-Real-Time SSM/I-SSMIS EASE-Grid Daily Global Ice Concentration and Snow Extent, 2008—2010. Boulder, Colorado USA: National Snow and Ice Data Center. Digital media

Perovich D K, Grenfell T C, Light B, Richter-Menge J A, Sturm M,

Tucker III W B, Eicken H, Maykut G A and Elder B. 1999a. SHEBA: Snow and Ice Studies [CD-ROM]. U. S. Army Cold Reg. Res. and Eng. Lab

Perovich D K, Andreas E L, Curry J A, Eiken H, Fairall C W, Grenfell T C, Guest P S, Intrieri J, Kadko D, Lindsay R W, McPhee M G, Morison J, Moritz R E, Paulson C A, Pegau W S, Persson P O G, Pinkel R, Richter-Menge J A, Stanton T, Stern H, Sturm M, Tucker III W B and Uttal T. 1999b. Year on ice gives climate insights. Eos Transactions American Geophysical Union, 80(41): 481 [DOI: 10.1029/EO080i041p00481-01]

Perovich D K, Grenfell T C, Light B and Hobbs P V. 2002. Seasonal evolution of the albedo of multiyear Arctic sea ice. Journal Geophysical Research 107(C10): 8044 [DOI: 10.1029/2000JC000438]

Persson P O G, Fairall C W, Andreas E L, Guest P S and Perovich D K. 2002. Measurements near the Atmospheric Surface Flux Group tower at SHEBA: Near-surface conditions and surface energy budget. Journal of Geophysical Research, 107(C10): 8045 [DOI: 10.1029/2000JC000705]

Schlesinger M E and Jiang X J. 1988. The transport of CO_2-induced warming into the ocean: An analysis of simulations by the OSU coupled atmosphere-ocean general circulation model. Climate D ynamics, 3(1): 1-17 [DOI: 10.1007/BF01089369]

Sellers W D. 1969. A global climate model based on the energy balance of the earth-atmosphere system. Journal of Applied Meteorology, 8(3): 392-400 [DOI: 10.1175/1520-0450(1969)008<0392:AGCMBO>2.0.CO;2]

Song J and Gao W. 1999. An improved method to derive surface albedo from narrowband AVHRR satellite data: narrowband to broadband conversion. Journal of Applied Meteorology, 38(2): 239-249 [DOI: 10.1175%2f1520-0450(1999)038%26lt%3b0239%3aAIMTDS%26gt%3b2.0.CO%3b2]

Stamnes K, Ellingson R G, Curry J A, Walsh J E and Zak B D. 1999. Review of science issues and deployment strategies for the north slope of Alaska/adjacent Arctic Ocean (NSA/AAO) ARM site. Journal of Climate, 12: 1413-1423

Stroeve J, Nolin A and Steffen T. 1997. Comparison of AVHRR derived and in situ surface albedo over the Greenland ice sheet. Remote Sensing of Environment, 62(3): 262-276 [DOI: 10.1016/S0034-4257(97)00107-7]

Sturm M, Maslanik J A, Perovich D K, Stroeve J C, Richter-Menge J, Markus T, Holmgren J, Heinrichs J F and Tape K. 2006. Snow depth and ice thickness measurements from the Beaufort and Chukchi Seas collected during the AMSR-Ice03 campaign. IEEE Transactions on Geoscience and Remote Sensing, 44(11): 3 009-3020

Valiente J A, Nunez M, Lopez-Baeza E and Moreno J F. 1995. Narrowband to broad-band conversion for Meteosat-visiible channel and broad-band albedo using both AVHRR-1 and -2 channels. International Journal of Remote Sensing, 16(6): 1147-1166

Wang J M and Gao F. 2004. Discussion on the problems on landsurface albedo retrieval by remote sensing data. Remote Sensing Technology and Application, 19(5): 295-300

Xiong X Z, Stammes K and Lubin D. 2002. Surface albedo over the Arctic ocean derived from AVHRR and its validation with SHEBA data. Journal of Applied Meteorology, 41: 413-425

Yu X G. 2011. The Report of 2010 Chinese Arctic Research Expedition. Beijing: Ocean Press

基于 NOAA/AVHRR 数据的北极反照率反演及其变化研究

王红燕，管磊，康立廷

中国海洋大学 海洋遥感研究所/信息科学与工程学院海洋技术系，山东 青岛 266100

摘　要: 极地海冰反照率直接影响极区的热收支，反照率的变化对地气系统热量收支平衡及气候变化等的研究具有重要意义。本文采用由美国国家海洋与大气管理局 NOAA (National Oceanic and Atmospheric Administration) 发射的 NOAA 卫星携带的先进的甚高分辨率辐射仪 AVHRR (Advanced Very High Resolution Radiometer) Level-1B (L1B) 数据，经宽带反射率转换、各向异性校正、大气订正、云检测等处理，得到 4 km 宽带晴空地表反照率产品。将 AVHRR 反照率与北冰洋地表热收支 SHEBA (Surface Heat Budget of the Arctic Ocean) 实验数据进行印证，印证结果显示在冰雪冻结期二者平均偏差为 -0.07，标准偏差为 0.05。本文处理了 2008 年—2010 年的 AVHRR 数据，结合第 4 次北极科学考察现场观测数据研究了北极冰面月平均反照率的变化，从降雪和冰脊两个方面分析了反照率的变化，结果显示反照率在冰雪融化过程中变化约为 0.3，变化较大且较为迅速，表面粗糙的多年冰海域和较为平滑的一年冰海域的反照率在雪融化时期变化约为 0.2 且变化相对缓慢。研究结果表明，由冰雪融化引起的反照率变化较为快速且幅度较大，是引起北极反照率变化的主导因素。

关键词: NOAA/AVHRR，北极，反照率，降雪，冰脊

中图分类号: TP79　　**文献标志码**: A

引用格式: 王红燕，管磊，康立廷. 2013. 基于 NOAA/AVHRR 数据的北极反照率反演及其变化研究. 遥感学报，17(3): 541 -552

Wang H Y, Guan L and Kang L T. 2013. Retrieval and analysis of Arctic albedo from NOAA/AVHRR data. Journal of Remote Sensing, 17(3): 541 -552

1　引　言

地表反照率是影响地气系统热量收支平衡的重要因子(Curry 等，1996; Stamnes 等，1999)，对于北极海冰，反照率作用尤其重要，模型结果显示夏季反照率降低 0.15—0.20 会导致永久冰的彻底消融(Maykut 和 Untersteiner，1971)。冰反照率正反馈机制(Budyko，1969; Sellers，1969; Schlesinger 和 Jiang，1988)说明了海冰覆盖与气候的密切关系，即全球气温的上升引起极地海冰量减小，北极海冰的消融速度加快，这种状况会导致北极海面反射的阳光越来越少，海面会吸收更多的阳光热量，这样的循环作用造成海冰不断融化。海冰对极地海洋和大气之间的热量和水汽交换的影响非常显著，极区海冰-反照率的反馈机制，对全球变暖具有放大作用，因而对极区冰面反照率的监测十分重要。

反照率是指地表在太阳辐射影响下，向上的反射辐射能量与向下的入射辐射能量的比值，其中向上及向下的辐射能量均包含了所有波段的辐射能量(Valiente 等，1995; Song 和 Gao，1999)。它与反射率概念不同，反射率是指某一波段向一定方向的反射，而反照率是反射率在所有方向上的积分，是遥感反演的重要地表参量，是反映地表对太阳短波辐射反射特性的物理参量，也是遥感反演陆面参数时的第一重要参数(王介民和高峰，2004)。获取冰雪反照率数据目前有两种方法: 现场测量和卫星遥感估算。用于冰雪反照率观测的卫星传感器主要是可见光红外波段传感器，其物理基础是辐射传输模型。卫星测量大多是在分离的、波段较窄的不连续波长范围进行，而地面反照率是包括所有波长范围(相

收稿日期: 2012-02-14; **修订日期**: 2012-09-05; **优先数字出版日期**: 2012-10-12

基金项目: 国家高技术研究发展计划重点项目(863 计划)(编号: 2008AA121701)

第一作者简介: 王红燕(1984—)，女，博士研究生，主要从事可见光红外卫星海洋遥感研究。E-mail: wanghongyan2011@gmail.com

通信作者简介: 管磊(1969—)，女，教授，主要从事卫星海洋遥感研究。E-mail: leiguan@ouc.edu.cn

当于宽带,一般为常用的总辐射计的测量范围)的积分,必须将以上所得到的各窄带反射率转化为宽带反照率(蒋熹,2006; Brandt 等, 2005; De Abreu 等, 1994; Valiente 等, 1995; Song 和 Gao, 1999; Xiong 等, 2002)。

2 数据介绍

2.1 卫星数据

NOAA/AVHRR 全球覆盖(Global Area Coverage, GAC) L1B 数据从 CLASS 系统(The Comprehensive Large Array-data Stewardship System)获取,数据分辨率为 4.4 km,每天约有 14 轨数据,AVHRR 光谱通道特征见表 1。CLASS 是 NOAA 环境数据库,数据可在线获取([2008 - 01 - 09] http://www.nsof.class.noaa.gov/saa/products/welcome)。

表 1 AVHRR 光谱通道特征

波段	1	2	3A	3B	4	5
波长/μm	0.58—0.68	0.725—1.000	1.58—1.64	3.55—3.93	10.3—11.3	11.5—12.5
信噪比(0.5% albedo)	≥9∶1	≥9∶1	≥20∶1	—	—	—
等效噪声温差(300 K)	—	—	—	≤0.12 K	≤0.12 K	≤0.12 K
温度范围/K	—	—	—	108—335	180—335	180—335

SSM/I(Special Sensor Microwave Imager)全球冰密集度及积雪覆盖数据为北极反照率反演的辅助数据,从美国国家冰雪数据中心 NSIDC(National Snow & Ice Data Center)获取,数据分辨率为 25 km(Nolin 等, 1998)([2008 - 01 - 09] http://nsidc.org/data/docs/daac/nise1_nise.gd.html#format)。

AMSR-E(Advanced Microwave Scanning Radiometer-Earth Observing System)积雪深度产品数据由 NSIDC 发布,数据分辨率为 12.5 km(Cavalieri 等, 2004)([2008 - 01 - 09] http://nsidc.org/data/ae_si12.html)。

2.2 现场观测数据

2.2.1 第 4 次北极科学考察现场测量数据

2010 年 7 月 1 号,"雪龙"号开启了中国第 4 次北极科学考察,考察历时 82 天,是中国历次北极考察时间最长的一次。"雪龙"号极地科学考察船总航行超过 12600 n mile,最北到达 88°26′N(余兴光, 2011)。期间,采用 Kipp & Zonen CMA6 进行了反照率测量,包括短期冰站工作和长期冰站工作,第 4 次北极考察 CMA6 测量实为 22 天的测量数据,测量日期从 2010 年 7 月 27 日至 2010 年 8 月 24 日。

短期冰站中,工作内容主要有融雪反照率和融池反照率的观测。反照率在冰面的测量尽量选在冰面比较平整、冰丘和融池影响不到的地方进行观测。反照率在融池的观测尽量将 CMA6 仪器放在融池内,减少融池边缘对观测的影响。

长期冰站中,工作内容主要为积雪厚度和反照率的观测。反照率的现场测量选在 200 × 125 m 的十字线上每隔 3 天观测一次,融雪反照率的观测间隔为 20 m。

2.2.2 SHEBA 数据

北冰洋地表热收支数据 SHEBA(Surface Heat Budget of the Arctic Ocean)是加拿大海岸警卫队破冰船 Des Groseilliers 航次上,在北冰洋波弗特海和楚科奇海浮冰上进行连续一年观测所获取的现场观测资料,浮冰运动里程达 1400 km,纬度跨越范围为 74° N—81° N(Perovich 等, 1999a; Persson 等, 2002)。期间采用 Kipp & Zonen 反照率仪在地表类型多样的冰站进行现场实测数据的采集。反照率现场测量选在一条 200 m 的线上每隔 2.5 m 测量一次,测量日期从 1997 年 10 月至 1998 年 10 月,测量精度为 ± 0.01(Perovich 等, 1999a; Perovich 等, 1999b; Perovich 等,2002)([2010 - 09 - 10] ftp://ftp1.esrl.noaa.gov/users/opersson/sheba/)。

2.3 研究区域

在降雪对反照率变化影响分析中,结合 NSIDC 发布的 AMSR-E 积雪深度数据,以区域(75° N,147°W)为中心选取 200 × 200 km 的研究区域,研究区域位置如图 1 中字母 A 所示。

为了研究冰脊对反照率变化的影响,分别在波弗特海域位置(75°N,128°W)和楚科奇海域位置(72°N,166°W)选取 200 × 200 km 的研究区域,波弗特海域多为多年冰分布,冰脊堆积,海冰表面较粗糙,且积雪深度较高;楚科奇海域大部分为一年冰分布,冰表面光滑,有少量冰脊分布(Sturm 等, 2006),研究区域位置如图 2 所示,其中 A 表示在波弗特海域中选取的研究区域,B 表示在楚科奇海域中选取的研究区域,图中白色代表云或无有效数据。

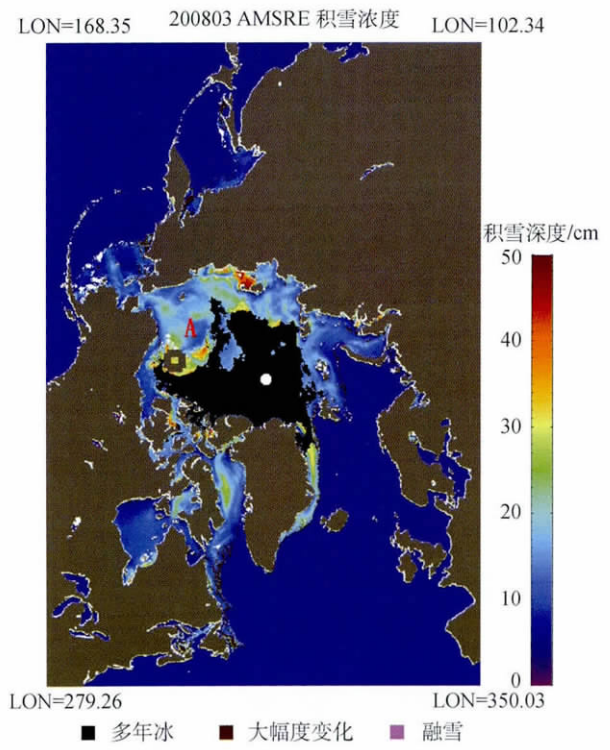

图 1 2008 年 3 月北极月平均积雪深度(A 为研究区域位置)

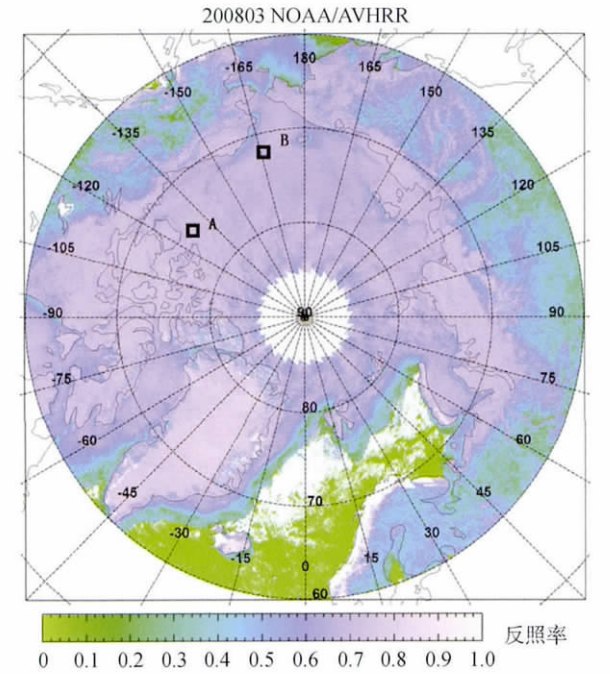

图 2 2008 年 3 月北极月平均反照率

(A:波弗特海域;B:楚科奇海域)

3 数据处理

Koepke (1989) 提出了 AVHRR 通道 1 和通道 2 地表窄带反照率和大气层顶反射率的线性关系。该线性关系对不同的气溶胶光学厚度、臭氧含量、水汽含量及太阳天顶角有不同的系数。基于 Koepke 的理论,不少学者利用 NOAA/AVHRR 数据对冰雪反照率进行了相关研究(De Abreu 等, 1994; Knap 和 Oerlemans, 1996; Knap 等, 1999; Stroeve 等, 1997; Li 和 Leighton, 1992; Lindsay 和 Rothrock, 1994) 。本文中反照率反演的处理过程包括太阳天顶角校正、宽带反射率转换、各向异性校正、大气订正 (Fowler 等, 2000) 以及云检测(Key, 1999) 。

太阳天顶角校正 AVHRR 的可见光与近红外通道(0.58—0.68 μm 和 0.725—1.000 μm) :

$$R_{1,\mathrm{toa}} = r_1/\cos(\theta) \quad (1)$$

$$R_{2,\mathrm{toa}} = r_2/\cos(\theta) \quad (2)$$

式中,$R_{1,\mathrm{toa}}$、$R_{2,\mathrm{toa}}$分别为校正后大气层顶可见光、近红外通道的反射率,r_1 为可见光通道的反射率,r_2 为近红外通道的反射率,θ 为太阳天顶角。窄带反射率到宽带反射率的转换为:

$$R_{\mathrm{toa}} = a + b \cdot R_{1,\mathrm{toa}} + c \cdot R_{2,\mathrm{toa}} \quad (3)$$

式中,R_{toa}为大气层顶宽带反射率,a,b,c 为转换系数。转换系数由辐射传输模型模拟得到,转换系数的获取需要考虑观测和照明角度、大气状况及地表类型、反照率等(Key 和 Schweiger,1998) 。当地表类型为海冰覆盖时,式(3) 为:

$$R_{\mathrm{toa}} = 0.022 + 0.277R_{1,\mathrm{toa}} + 0.507R_{2,\mathrm{toa}} \quad (4)$$

各向异性订正:

$$A_{\mathrm{toa}} = R_{\mathrm{toa}}/f \quad (5)$$

式中,A_{toa}为大气层顶宽带反照率,f 为各向异性反射率因子。大气校正:

$$A_{\mathrm{surface}} = (A_{\mathrm{toa}} - m)/n \quad (6)$$

式中,A_{surface}为地表反照率,m、n 为水汽、气溶胶含量、太阳天顶角的函数。

云检处理方法基于云和地表参数反演系统 CASPR(Cloud and Surface Parameter Retrieval System) 提供的云检算法(Key, 1999) ,CASPR 提供的云检算法主要有 5 个云检测试: (1) 卷云测试(11—12 μm) 主要针对冰、海洋和陆地进行测试; (2) 暖云测试(11—12 μm) 针对所有地表类型进行测试; (3) 水汽云测试(3.7 μm) 针对海洋和陆地; (4) 冷云测试 (11 μm) 针对所有地表类型; (5) 晴空测试针对冰和雪。经过云检处理后的北极反照率结果如图 3 所示,图中不同颜色表示不同的地表反照率值,白色代表云或无有效数据。

第 4 次北极科学考察实测数据受云影响较为严

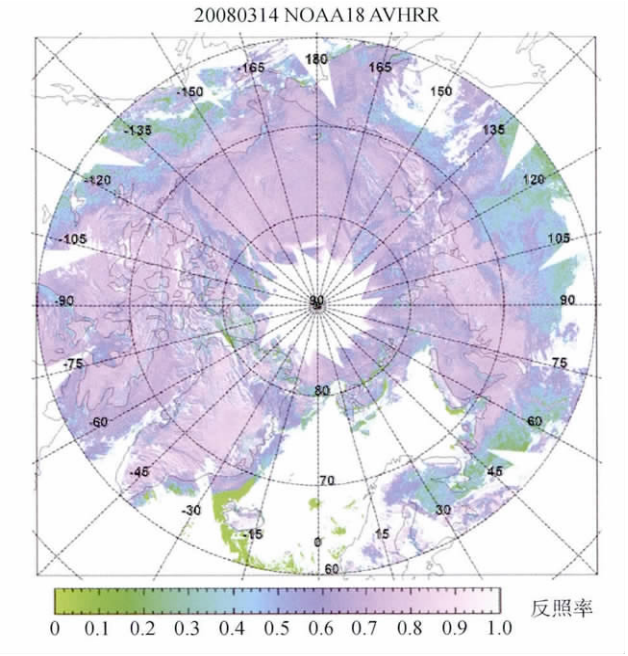

图3 2008 年 3 月 14 日北极反照率

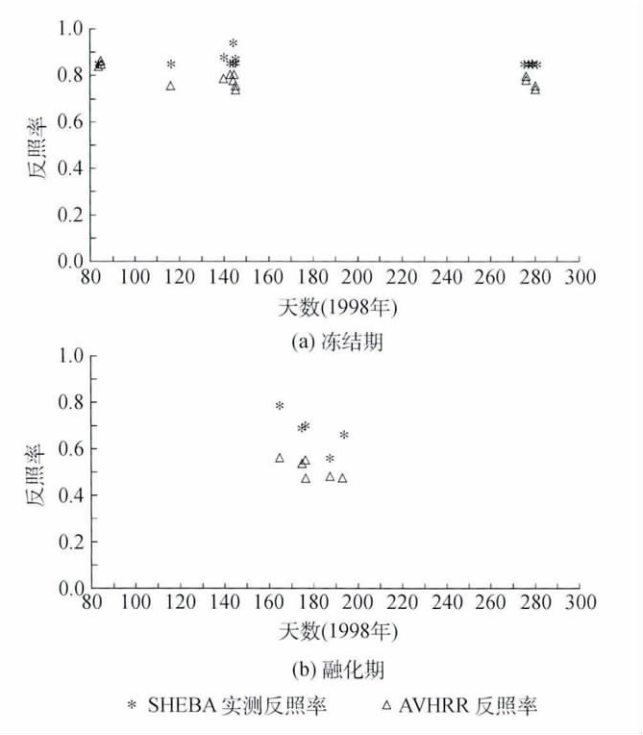

图4 反照率印证

重,导致与 AVHRR 反照率数据无相匹配的数据,改用 SHEBA 实验获取的历史实测数据进行 AVHRR 反照率数据印证。根据 SHEBA 实测数据的现场观测记录,4、5 月份为干雪阶段,反照率观测值较高约为 0.84,随后从 5 月末到 8 月中旬有 80 天的融化期,8 月 12 日反照率值达到夏季融化期最低值,8 月末积雪开始在冰上堆结,到 9 月中旬积雪深度达到 10 cm(Curry 等,2001)。将 SHEBA 与 AVHRR 反照率在冰雪冻结期(3 月—5 月,10 月)和冰雪融化期(6 月—9 月)分别进行匹配处理,空间为 4 km,时间窗口为 2 h,得到 28 对匹配点(图 4),其中冰雪冻结期有 22 对,冰雪融化期有 6 对。印证结果显示,在冰雪冻结期二者平均偏差为 -0.07(AVHRR-SHEBA),标准偏差为 0.05;在冰雪融化期 6 对匹配点偏差范围在 -0.23— -0.08,平均偏差为 -0.17。冰雪冻结期由于地表类型较为均一,二者差异较小;在冰雪融化时期地表类型较为复杂,二者差异比较显著,在卫星覆盖的 4 km 范围内可能存在融雪、融池等多种地表类型,现场测量的地表类型与卫星观测的地表类型很难匹配,导致二者反照率差异较大。

4 反照率变化分析

本文按照上述算法处理了 2008 年至 2010 年的 AVHRR 数据,并由日平均数据处理得到月平均数据,结合中国第 4 次北极科学考察现场观测的 CMA6 反照率实测数据分析了北极地表反照率的变化。北极地表反照率变化经过 5 个阶段(5 月—8 月为过渡季节)(Curry 和 Schramm,1995; Laine,2004; Perovich 等,2002; Xiong 等,2002):(1)干雪阶段:4 月—5 月为干雪阶段,此时反照率较高,可达 0.8—0.9,地表类型较为复杂;(2)融雪阶段:5 月末降雪停止,反照率值降到沉积雪的反照率值,几天以后,积雪开始融化,反照率值降到融雪时的值;(3)融池的形成:7 月中旬积雪融化,由于融池的形成在短短一周内会引起反照率突然下降;(4)融池的发展:在第 3 阶段以后积雪继续融化,除了厚冰覆盖的地方外,雪融化到只剩下裸露的冰,当融池面积达到最大的时候,反照率降到一年来的最低值;(5)秋季冻结:8 月份融池逐渐开始结冰,反照率值逐渐升到裸露冰的反照率值,水道也开始冻结。积雪在 9 月开始堆积,反照率值逐渐回升到新雪时的值。本文首先从第 4 次北极科学考察实测数据来看不同地表类型的反照率变化,新雪的反照率较高约为 0.8—0.9,融雪反照率略低约为 0.6,融池反照率约 0.1—0.2,从不同地表类型的 CMA6 实测数据的变化来看,随着冰雪融化过程反照率逐渐降低,反照率的变化与 Lindsay 和 Rothrock(1994)的结果一致。从降雪和冰脊两个方面来分析反照率的变化,在降雪

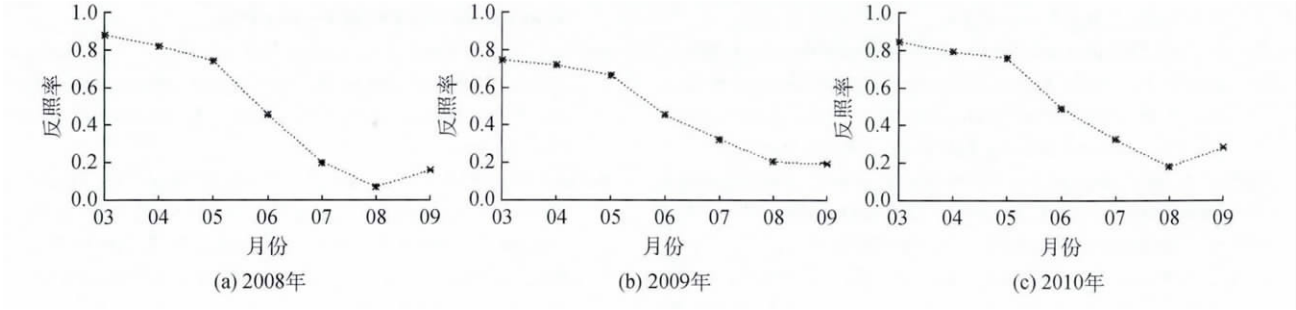

图 5 2008 年—2010 年在降雪区域内反照率变化曲线

对反照率变化影响分析中,在图 1 所标注的研究区域内做 2008 年、2009 年和 2010 年 3 月—9 月的 AVHRR 月平均反照率变化分析,结果如图 5 所示。从曲线图中看到 3 月、4 月反照率约为 0.7—0.8,此时北极多为冰雪;5 月末积雪开始融化,反照率降低至 0.66—0.75,随着积雪进一步融化,6 月反照率继续降低至约 0.45,在 8 月当融池分布达到最广时反照率降至最低,9 月末融池开始冻结,反照率逐渐回升,反照率在冰雪融化过程中变化约为 0.3 且变化较为迅速。

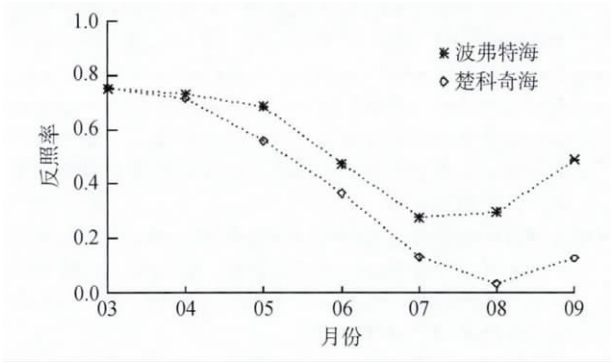

图 6 波弗特海和楚科奇海 2009 年反照率变化曲线

为研究冰脊对反照率变化的影响,在图 2 所示的研究区域对 AVHRR 月平均反照率变化进行分析,2009 年 3 月—9 月 AVHRR 反照率变化曲线图如图 6 所示,从曲线图中看到 3 月、4 月两个研究区域反照率值近似相同约为 0.75,此时北极多为冰雪;5 月末冰雪开始融化,反照率开始降低,此时波弗特海区域反照率约为 0.68,楚科奇海区域反照率约为 0.56,6 月冰雪融化,波弗特海区域反照率约为 0.47,楚科奇海区域反照率约为 0.37,7 月冰雪继续融化,波弗特海区域反照率约为 0.28,楚科奇海区域反照率约为 0.13,在 8 月当融池分布最广时反照率降至全年最低,9 月融水开始冻结,反照率逐渐回升,反照率在冰雪融化过程中相差约 0.2 且变化相对缓慢。

5 结 论

本文采用 NOAA/AVHRR GAC L1B 数据,经宽带反射率转换、各向异性校正、大气订正、云检测等处理,得到 4 km 晴空宽带地表反照率产品。将 AVHRR 反照率与 SHEBA 实测数据进行比较,印证结果显示在冰雪冻结期二者平均偏差为 -0.07,标准偏差为 0.05,结果较好。采用 2008 年到 2010 年的 AVHRR 数据,结合中国第 4 次北极科学考察现场观测数据研究了北极冰面反照率的变化。从降雪和冰脊两个方面来分析反照率的变化,在降雪对反照率变化影响分析中,研究结果显示反照率在冰雪融化过程中变化约为 0.3 且变化较为迅速。在冰脊对反照率变化的影响研究中,分别在波弗特海域和楚科奇海域选取研究区域,2009 年 3 月—9 月这两个研究区域中的 AVHRR 月平均反照率变化曲线结果显示反照率在冰雪融化过程中变化相对缓慢,两个区域相差约 0.2。从降雪和冰脊对反照率变化的分析结果来看,由冰雪融化引起的反照率变化较快且幅度较大,是引起北极反照率变化的主导因素。

志 谢 NOAA/AVHRR 数据由美国 CLASS 提供,SSM/I 数据和 AMSR-E 数据由 NSIDC 提供,反照率实测数据来自中国第 4 次北极科学考察和 SHEBA 实验,在此表示衷心感谢。

参考文献(References)

Brandt R E, Warren S G, Worby A P and Grenfell T C. 2005. Surface albedo of the Antarctic sea ice zone. Journal of Climate, 18(17): 3606 - 3622 [DOI: 10.1175/JCLI3489.1]

Budyko M I. 1969. The effect of solar radiation variations on the climate of the earth. Tellus, 21: 611 - 619

Cavalieri D J, Markus T and Comiso J. 2004. Updated daily. AMSR-E/Aqua Daily L3 12.5 km Brightness Temperature, Sea Ice Conentration, & Snow Depth Polar Grids V002, 2008—2010. Boulder, Colorado USA: National Snow and Ice Data Center. Digital media

Curry J A and Schramm J L. 1995. Sea ice-albedo climate feedback mechanism. Journal of Climate, 8(2): 240 – 247 [DOI: 10.1175/1520 – 0442(1995)008 <0240: SIACFM >2.0.CO;2]

Curry J A, Rossow W B, Randall D and Schramm J L. 1996. Overview of Arctic cloud and radiation characteristics. Journal of Climate, 9(8): 1731 – 1764 [DOI: 10.1175/1520 – 0442(1996) 009 <1731: OOACAR >2.0.CO;2]

Curry J A, Schramm J L, Perovich D K and Pinto J O. 2001. Applications of SHEBA/FIRE data to evaluation of snow/ice albedo parameterizations. Journal of Geophysical Research: Atmospheres, 106(D14): 15345 – 15355 [DOI: 10.1029/2000JD 900311]

De Abreu R A, Key J, Maslanik J A, Serreze M C and LeDrew E F. 1994. Comparison of in situ and AVHRR-derived broadband albedo over Arctic sea ice. Arctic, 47(3): 288 – 297

Fowler C, Maslanik J, Haran T, Scambos T, Key J and Emery W. 2000. AVHRR Polar Pathfinder twice-daily 5 km EASE-grid Composites. http://nsidc.org/data/nsidc-0066.html, Natl. Snow and Ice Data Cent., Boulder, Colo

蒋熹. 2006. **冰雪反照率研究进展**. **冰川冻土**, 28(5): 728 – 736

Key J. 1999. The Cloud and Surface Parameter Retrieval (CASPR) System for Polar AVHRR. Cooperative Institute for Meteorological Satellite Studies. University of Wisconsin, Madison

Key J and Schweiger A J. 1998. Tools for atmospheric radiative transfer: *streamer* and *FluxNet*. Computers and Geosciences, 24(5): 443 – 451 [DOI: 10.1016/S0098 – 3004(97)00130 – 1]

Knap W H and Oerlemans J. 1996. The surface albedo of the Greenland ice sheet: satellite-derived and in situ measurement in the Sondre Stromfjord and during the 1991 melt season. Journal of Glaciology, 42: 364 – 374

Knap W H, Brock B W, Oerlemans J and Wills I C. 1999. Comparison of Landsat TM-derived and ground-based albedos of Hunt Glacier d'Arolla, Switzerland. International Journal of Remote Sensing, 20: 3293 – 3310

Koepke P. 1989. Removal of atmospheric effects from AVHRR albedos. Journal of Applied Meteorology, 28(12): 1344 – 1348 [DOI: 10.1175/1520 – 0450(1989)028 <1341: ROAEPA >2.0.CO;2]

Laine V. 2004. Arctic sea ice regional albedo variability and trends. Journal of Geophysical Research, 109(C06027): 1982 – 1998 [DOI: 10.1029/2003JC001818]

Li Z Q and Leighton H G. 1992. Narrowband to broadband conversion with spatially autocorrelated reflectance measurement. Journal of Applied Meteorology, 31(5): 421 – 433 [DOI: 10.1175/1520 – 0450(1992)031 <0421: NTBCWS >2.0.CO;2]

Lindsay R W and Rothrock D A. 1994. Arctic sea ice albedo from AVHRR. Journal of Climate, 7(11): 1737 – 1749 [DOI: 10.1175%2f1520 – 0442(1994)007%3c1737%3aASIAFA%3e2.0.CO%3b2]

Maykut G A and Untersteiner N. 1971. Some results from a time dependent, thermodynamic model of sea ice. Journal of Geophysical Research, 76(6): 1550 – 1575 [DOI: 10.1029/JC076i006p01550]

Nolin A, Armstrong R L and Maslanik J. 1998. Updated daily. Near-Real-Time SSM/I-SSMIS EASE-Grid Daily Global Ice Concentration and Snow Extent, 2008—2010. Boulder, Colorado USA: National Snow and Ice Data Center. Digital media

Perovich D K, Grenfell T C, Light B, Richter-Menge J A, Sturm M, Tucker III W B, Eicken H, Maykut G A and Elder B. 1999a. SHEBA: Snow and Ice Studies [CD-ROM]. U. S. Army Cold Reg. Res. and Eng. Lab

Perovich D K, Andreas E L, Curry J A, Eiken H, Fairall C W, Grenfell T C, Guest P S, Intrieri J, Kadko D, Lindsay R W, McPhee M G, Morison J, Moritz R E, Paulson C A, Pegau W S, Persson P O G, Pinkel R, Richter-Menge J A, Stanton T, Stern H, Sturm M, Tucker III W B and Uttal T. 1999b. Year on ice gives climate insights. Eos Transactions American Geophysical Union, 80(41): 481 [DOI: 10.1029/EO080i041p00481 – 01]

Perovich D K, Grenfell T C, Light B and Hobbs P V. 2002. Seasonal evolution of the albedo of multiyear Arctic sea ice. Journal Geophysical Research 107(C10): 8044 [DOI: 10.1029/2000JC000438]

Persson P O G, Fairall C W, Andreas E L, Guest P S and Perovich D K. 2002. Measurements near the Atmospheric Surface Flux Group tower at SHEBA: Near-surface conditions and surface energy budget. Journal of Geophysical Research, 107(C10): 8045 [DOI: 10.1029/2000JC000705]

Schlesinger M E and Jiang X J. 1988. The transport of CO_2-induced warming into the ocean: An analysis of simulations by the OSU coupled atmosphere-ocean general circulation model. Climate D ynamics, 3(1): 1 – 17 [DOI: 10.1007/BF01089369]

Sellers W D. 1969. A global climate model based on the energy balance of the earth-atmosphere system. Journal of Applied Meteorology, 8(3): 392 – 400 [DOI: 10.1175/1520 – 0450(1969)008 <0392: AGCMBO >2.0.CO;2]

Song J and Gao W. 1999. An improved method to derive surface albedo from narrowband AVHRR satellite data: narrowband to broadband conversion. Journal of Applied Meteorology, 38(2): 239 – 249 [DOI: 10.1175%2f1520 – 0450(1999)038%26lt%3b0239%3aAIMTDS%26gt%3b2.0.CO%3b2]

Stamnes K, Ellingson R G, Curry J A, Walsh J E and Zak B D. 1999. Review of science issues and deployment strategies for the north slope of Alaska/adjacent Arctic Ocean (NSA/AAO) ARM site. Journal of Climate, 12: 1413 – 1423

Stroeve J, Nolin A and Steffen T. 1997. Comparison of AVHRR derived and in situ surface albedo over the Greenland ice sheet. Remote Sensing of Environment, 62(3): 262 – 276 [DOI: 10.1016/S0034 – 4257(97)00107 – 7]

Sturm M, Maslanik J A, Perovich D K, Stroeve J C, Richter-Menge J, Markus T, Holmgren J, Heinrichs J F and Tape K. 2006. Snow depth and ice thickness measurements from the Beaufort and Chukchi Seas collected during the AMSR-Ice03 campaign. IEEE Transactions on Geoscience and Remote Sensing, 44(11): 3009 – 3020

Valiente J A, Nunez M, Lopez-Baeza E and Moreno J F. 1995. Narrowband to broad-band conversion for Meteosat-visiible channel and broad-band albedo using both AVHRR-1 and -2 channels. International Journal of Remote Sensing, 16(6): 1147 – 1166

王介民, 高峰. 2004. **关于地表反照率遥感反演的几个问题** [J]. **遥感技术与应用**, 19(5): 295 – 300

Xiong X Z, Stammes K and Lubin D. 2002. Surface albedo over the Arctic ocean derived from AVHRR and its validation with SHEBA data. Journal of Applied Meteorology, 41: 413 – 425

余兴光. 2011. **中国第四次北极科学考察报告**. **北京: 海洋出版社**